metals

MDPI

Article

Picosecond Laser Shock Peening of Nimonic 263 at 1064 nm and 532 nm Wavelength

Sanja Petronic [1,*,†], Tatjana Sibalija [2,†], Meri Burzic [1], Suzana Polic [3], Katarina Colic [1] and Dubravka Milovanovic [4,†]

1 Innovation Center, Faculty of Mechanical Engineering, University of Belgrade, Kraljice Marije 16, 11000 Belgrade, Serbia; mburzic@mas.bg.ac.rs (M.B.); kbojic@mas.bg.ac.rs (K.C.)
2 Faculty of Information Technology, Faculty of Management, Metropolitan University, Tadeusa Koscuska 63, 11000 Belgrade, Serbia; tsibalija@gmail.com
3 Central Institute for Conservation in Belgrade, Terazije 26, 11000 Belgrade, Serbia; suzanapolic64@gmail.com
4 Vinca Institute of Nuclear Sciences, University of Belgrade, PO Box 522, 11001 Belgrade, Serbia, dubravka.milovanovic@vinca.rs
* Correspondence: sanjapetronic@yahoo.com; Tel.: +3-816-246-2922; Fax: +3-811-1337-0364
† These authors contributed equally to this work.

Academic Editor: Patrice Peyre
Received: 12 November 2015; Accepted: 5 February 2016; Published: 23 February 2016

Abstract: The paper presents a study on the surface modifications of nickel based superalloy Nimonic 263 induced by laser shock peening (LSP) process. The process was performed by Nd^{3+}:Yttrium Aluminium Garnet (YAG) picosecond laser using the following parameters: pulse duration 170 ps; repetition rate 10 Hz; pulse numbers of 50, 100 and 200; and wavelength of 1064 nm (with pulse energy of 2 mJ, 10 mJ and 15 mJ) and 532 nm (with pulse energy of 25 mJ, 30 mJ and 35 mJ). The following response characteristics were analyzed: modified surface areas obtained by the laser/material interaction were observed by scanning electron microscopy; elemental composition of the modified surface was evaluated by energy-dispersive spectroscopy (EDS); and Vickers microhardness tests were performed. LSP processing at both 1064 nm and 532 nm wavelengths improved the surface structure and microhardness of a material. Surface morphology changes of the irradiated samples were determined and surface roughness was calculated. These investigations are intended to contribute to the study on the level of microstructure and mechanical properties improvements due to LSP process that operate in a picosecond regime. In particular, the effects of laser wavelength on the microstructural and mechanical changes of a material are studied in detail.

Keywords: laser modification; Nd:YAG; shock peening; Nimonic; superalloy

1. Introduction

Nickel based superalloys are materials with remarkable combination of mechanical and physical properties that contribute to their wide application, from gas turbine, aero and rocket engines to chemical processing plants, as presented by Pollock and Tin [1]. Nimonic alloys are the group of Ni-based superalloys, which are widely used for high performance applications, such as disks and blades of either aircraft engines or land-based gas turbines, at temperatures ranging from 650 °C to 1050 °C and in aggressive atmospheres [2]. Nimonic alloy 263 is an important precipitation hardening nickel base superalloy, with high creep strength and oxidation resistance, designed for stationary components like combustion chambers, casings, liners, exhaust ducting, bearing housings and many others [3]. Since the components of this alloy are primarily degraded by creep damage, as presented by Park *et al.* [4], when it is exposed to the influence of harsh environment, it is necessary to retard intergranular cracking and propagation for better performance at elevated temperatures.

Lasers have been used for high precision material processing in micro- and nano-manufacturing operations due to a specific nature of the laser light, high intensity and possibility of controlled surface modification. In the last few decades, surface modifications of different metals and their alloys performed by various types of lasers has gained significant attention. Milanovic *et al.* [5] presented the surface modification of titanium based implant by picosecond laser at both 1064 nm and 532 nm, and found periodic surface structures. Treatment of nickel based superalloys' surfaces by laser irradiation can induce specific changes in the microstructure, which result in improved mechanical properties of the material, as discussed by Petronic *et al.* [6].

The principle of laser shock peening (LSP) implies usage of high intensity laser beam and suitable overlays to generate high pressure shock waves on the surface of a workpiece. Laser shock processing of steel was studied by Yilbas *et al.* [7]. They showed that dislocations are governing mechanism in hardening of the alloy, and the hardness of peened alloy increased 1.7 times compared to the base material. A review on laser shock processing was carried out by Peyre and Fabbro [8]. They presented physical principles of laser shock and induced mechanical effects, and found that higher pressures can be achieved with confinement as compared to direct ablation.

Laser shock processing of metallic surfaces and its applications were presented by Devaux *et al.* [9], theoretically and experimentally. The transient shock waves induce microstructure changes near the surface and alter the stress level, which improve the mechanical properties of material, such as hardness and fatigue strength. Peyre *et al.* [10] presented analytical models for the confined ablation, plastically affected depths and residual stresses induced at the surface. Hong and Chengye [11] showed the improvement in fatigue strength due to the surface residual stresses, while Clauer and Holbrook [12] showed that improvement in hardness is the result of dislocations and other phases' formation arisen by laser shock peening. During LSP process strain rates could reach as high as 10^6 s^{-1}, which is very high compared to the conventional strain rates. Amarchinta *et al.* [13] used a finite element technique to predict the residual stresses induced by LSP process, which was followed by comparison between experimental results and simulation. Peyre *et al.* [14] demonstrated that a finite element modeling procedure could be successfully applied to the prediction of residual stresses induced by laser shock processing. Sibalija *et al.* [15] used a hybrid designed method, based on the artificial intelligence techniques, to optimize LSP parameters in order to improve several characteristics of the processed Nimonic 263 sheets: surface characteristics, microstructure, roughness, microhardness and microstructural transformations.

The beneficial effects of LSP include improvement of microstructure, surface quality, *etc.*, which delays the fatigue crack initiation. The surface morphology of metals has a great effect on fatigue behavior, and many laser peened materials showed improvements in fatigue life with LSP, as shown by Ding and Ye [16]. Surface condition has considerable influence on fatigue strength, and the following factors have the most significant effects: surface roughness, residual stresses in the surface layer, work hardening or softening in the surface layer, and change or transformation of the microstructure due to plastic deformation, as presented by Schijve [17].

Although in the last few decades many investigations were devoted to the laser shock peening, most of them were performed in nanosecond laser beam regime. Since the invention of laser, there has been a constant development in terms of shorter pulse times. Some investigation were carried out in femtosecond regime [18,19], including the effect of wavelength on the microstructure characteristics [20]. There is an emerging interest in employing picosecond laser for LSP application, but picosecond laser regime has been rarely discussed in the literature. Therefore, this paper aims to contribute to the investigation of the microstructure features introduced by picosecond LSP. The investigation includes analysis of surface condition after LSP of material, discussion of microstructural changes arisen by the laser treatment, and microhardness testing after LSP. In particular, the impact of 1064 and 532 nm laser irradiation of the superalloy is discussed in detail. The rest of the paper is organized as follows. After the introduction, the experimental set up is presented in the second section. Results of the experiment are presented, analyzed and discussed in the third

section, which is divided into three parts: (i) discussion of the microstructural and surface changes arisen by 1064 nm wavelength laser beam; (ii) discussion of the microstructural and surface changes arisen by 532 nm wavelength laser beam; and (iii) comparison of influence of these two wavelengths on the microstructure. The last section brings the main and most important conclusions from the above analysis.

2. Experimental Section

Samples of superalloy Nimonic 263, prepared in the form of sheets with dimensions 10 mm × 50 mm × 1 mm, were polished and cleaned with ethanol prior to application of the protective layer. The chemical composition of Nimonic 263 is listed in Table 1.

Table 1. Chemical composition of alloy Nimonic 263.

Element	C	Si	Mn	Al	Co	Cr	Cu	Fe	Mo	Ti	Ni
%	0.06	0.3	0.5	0.5	20	20	0.1	0.5	5.9	2.2	49.94

The sample sheets were coated with black paint (protective overlay) and immersed in distilled water, which served as the transparent layer. The laser beam was guided by the mirror system and focused below the surface of the sample, at the incidence angle of 90°. The experimental setup for LSP processing of the Nimonic 263 samples is presented in Figure 1.

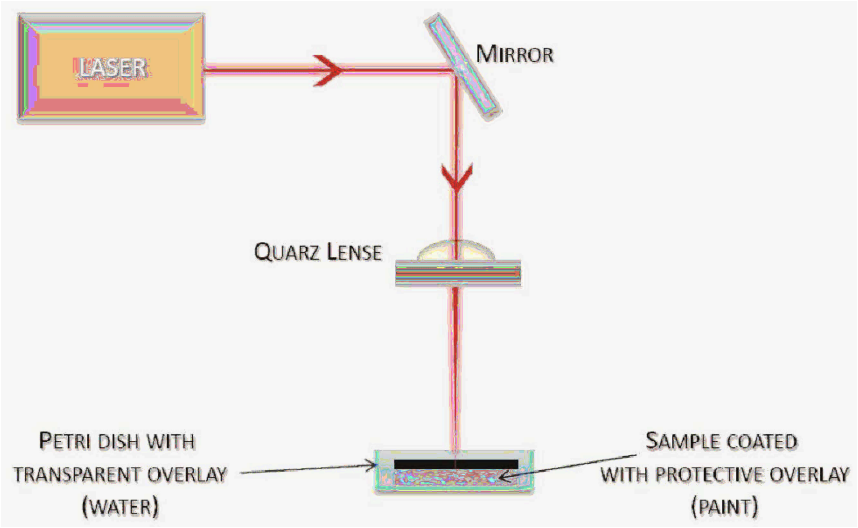

Figure 1. The experimental setup for laser shock peening.

The samples were exposed to a laser light at 1064 nm and 532 nm wavelength, with number of accumulated pulses: 50, 100 and 200. The operating laser was Nd:YAG EKSPLA, model SL212P, (Ekspla, Vilnius, Lithuania). At 1064 nm wavelength, pulse energies were varied from 2 mJ to 15 mJ and corresponding fluencies ranged from 0.1 to 0.3 J·cm^{-2}. At laser wavelength of 532 nm, pulse energies were varied from 20 to 35 mJ; corresponding fluencies ranged from 0.28 to 0.4 J·cm^{-2}. The spatial distribution of laser energy for both 1064 nm and 532 nm wavelengths is non-homogeneous. Specifically, the highest value of laser energy is at the center of the beam, and energy is decreasing at periphery of the beam. Characteristics of the picosecond laser used in this experiment are listed in Table 2.

surface effects strongly depend on the specific parameters of the operating laser (wavelength, pulse duration, energy, *etc.*) and surface conditions of the sample (roughness, absorbance coefficient, *etc.*). Treatment of a surface by the pulsed laser light with picosecond pulse duration can be accompanied by the formation of liquid phase which can decrease the precision of processing, as discussed by Bauerle [24]. The protective overlay in laser surface treatment of alloys is used for two reasons: (1) to absorb the incident laser energy, expand abruptly and transfer the shock wave to the metal target; and (2) to protect the metal target from the excessive heat influence of the incident light. The implementation of the transparent layer increases the plasma pressure by a trapping-like effect on the plasma expansion.

The transient shock waves induce microstructure changes near the surface and cause high density of dislocations to be formed. The combined effect of the microstructure changes and dislocation entanglement contributes to an increase in the mechanical properties near the surface. LSP improves fatigue, corrosion and wearing resistance of metals through mechanical effect produced by shock waves [25].

It is important to determine how protective layer influences the value of absorptivity/reflectivity of the sample surface for light wavelengths that were used in this experiment (532 nm and 1064 nm). Comparative reflectance spectra and the results for Nimonic 263 surface with and without protective paint are presented in Figure 3 and Table 3.

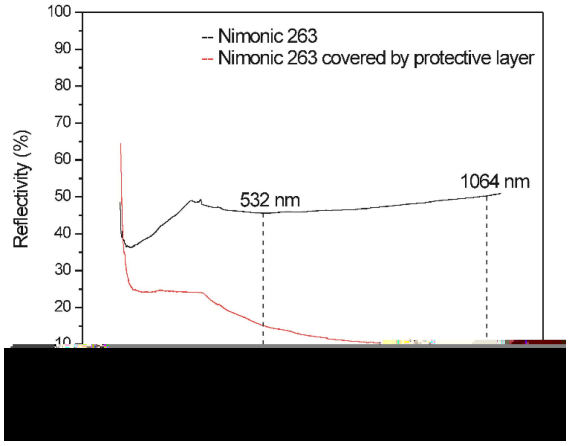

Figure 3. Comparative reflectance spectra of Nimonic 263 surface with and without protective paint layer.

The reflectivity of base material at 532 nm wavelength is lower than at 1064 nm, as shown in Figure 3. After applying the protective paint layer, surface of the sample covered by protective layer exhibits significantly lower values of reflectivity for incoming light than the sample base material, at both observed wavelengths. For 532 nm wavelength, the reflectance decreases by two-thirds, and for 1064 nm wavelength the value of reflectance reduces by four-fifths, as presented in Table 3.

Table 3. Reflectivity of Nimonic 263 with and without protective paint layer.

Wavelength (nm)	Reflectivity (%)	
	Nimonic 263	Nimonic 263 with protective layer
532	45.6	15.0
1064	50.2	9.8

The laser shock peening experiment was carried out with variation of pulse energy: 2 mJ, 10 mJ and 15 mJ at 1064 nm wavelength (respectively, power density values 0.7, 3.3 and 5 GW/cm^2), and 20 mJ, 25 mJ and 30 mJ at 532 nm wavelength (respectively, power density values 1.9, 2.4 and

2.8 GW/cm^2. Beside the pulse energy, the number of pulses was varied as well: 50, 100 and 200, for both groups of experiment.

3.1. Laser Shock Peening of Nimonic 263 at 1064 nm Wavelength

Figure 4 presents the microstructure after picosecond LSP process by the laser light at 1064 nm wavelength, pulse energy of 10 mJ and number of pulses 50, 100 and 200, respectively. When the number of accumulated pulses is increased, the microstructure becomes finer, but after 200 pulses the partial melting of the material occurs (Figure 4c), as the paint was partially removed. For this reason, LSP becomes a thermomechanical process (so called "direct ablation"), as presented in [26].

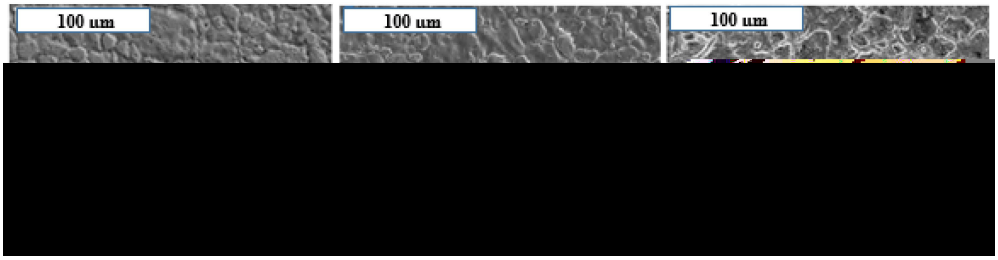

Figure 4. The microstructure of Nimonic 263 after LSP by laser pulse energy of 10 mJ (F = 0.2 J· cm^{-2}), wavelength of 1064 nm, and number of pulses 50 (**A**); 100 (**B**) and 200 (**C**), respectively (power density 3.3 GW/cm^2).

At 1064 nm laser action, the pulse energy values were 2 mJ, 10 mJ and 15 mJ, and the number of pulses 50, 100 and 200. The finest microstructure was obtained at pulse energy of 10 mJ (presented in Figure 4), as pulse energy of 15 mJ induced not only mechanical but thermal changes as well. Increase in the pulse energy leads to decrease of the grains size.

LSP is not a thermal but a mechanical process for treating materials, as Berthe *et al.* [27] presented in their work. This process is accompanied by significant changes in microstructures and phases near the surface. The mechanism of microstructure changes is similar to those arisen during the laser shoot peening. According to [28,29], after the deformation the grain size decreases due to sliding mechanism and hardening deformation. When the peak pressure of the shock wave exceeds the dynamic yield strength of alloys or metallic materials, plastic deformation occurs, resulting in the improvement of the near-surface microstructure and mechanical properties, which is accompanied by significant changes in microstructures and phases. Shock waves can produce one or the combination of the following metallurgical effects: generation of point defects, dislocations and twins, phase transformations and precipitation [30,31]. The changes in microstructure, induced by laser beam action, are typical for this superalloy and can be summarized as formation of carbides, TiC, CrC and (Ti, Mo)C, that segregate both at the grains and at the grain boundaries [32].

Titanium monocarbide (TiC) is very hard, stable at both high and low temperatures. (Ti, Mo)C is characteristic structural component that strongly influences mechanical and physical properties of material, as discussed by Chena *et al.* [33] and Jang *et al.* [34]. SEM microphotographs shown in Figure 5 present phases occurring after 1064 nm picosecond LSP, 10 mJ laser beam energy and pulse number of 100 (Figure 5a,b) and 50 (Figure 5c,d).

Table 4 shows the results of EDS analysis of the microconstituents denoted in Figure 5. These results suggest formation of various phases, both desirable and undesirable, depending on their morphology, size and the place/area of appearance. According to EDS results in Spectrum 1 and 3, as well as morphology of these phases which is rather regular pyramid, it can be assumed these phases are Ti carbides.

According to Table 4 and EDS results, carbides in Spectrum 2 and 4 are TiMo carbides. These types of compounds are characterized by the irregular shape and micrometer scale dimensions [34]. In this case, the presence of TiMo carbides is undesirable because their presence can cause the crack formation in the material.

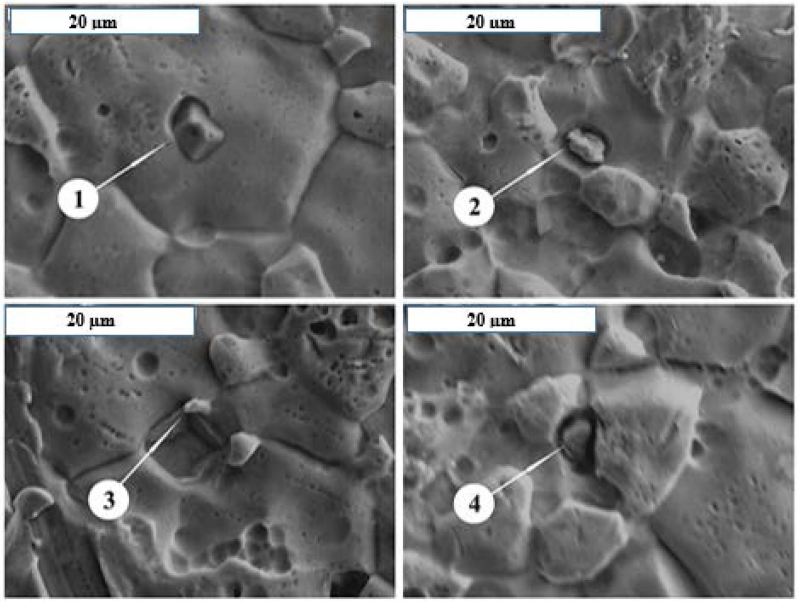

Figure 5. SEM of the microconstituents formed during LSP at 1064 nm, E = 10 mJ, and number of accumulated pulses: (**a**) 100; (**b**) 100; (**c**) 50 and (**d**) 50. Power density: 3.3 GW/cm^2.

Table 4. EDS analysis of the spots denoted in Figure 5.

Spectrum	C	Al	Si	Ti	Cr	Mn	Fe	Co	Ni	Mo
Spectrum 1	11.79	0.11	0.15	49.87	6.96	0.20	0.19	7.41	18.79	4.52
Spectrum 2	14.56	0.13	0.19	13.36	11.56	1.00	0.33	13.22	34.04	12.19
Spectrum 3	12.84	0.25	0.20	4.67	14.25	0.54	0.30	16.82	44.75	5.38
Spectrum 4	18.29	1.02	0.94	21.59	9.62	0.35	0.24	10.67	27.73	9.54

3.2. Laser Shock Peening of Nimonic 263 at 532 nm Wavelength

LSP is performed with the action of laser light at 532 nm wavelength, as well. Figure 6 shows the microstructure of Nimonic 263 obtained by the stated wavelength, 25 mJ energy and 50, 100 and 200 number of accumulated pulses, respectively. In contrast to the 1064 nm wavelength, the pulse energy of 2 mJ, 10 mJ and 15 mJ could not be applied with the wavelength of 532 nm, as it does not produce sufficient fluence required to make changes in a surface layer. When the pulse energy is increased, the pores start to form, while the increase in the number of applied pulses results in a "coral" structure, as shown in Figure 6. The grain boundaries are more pronounced with higher number of applied pulses. Unlike the treatment with the wavelength of 1064 nm, melting did not occur after 200 pulses (Figure 6c).

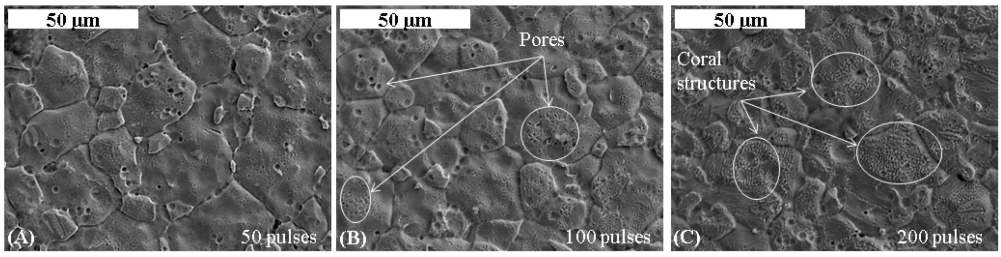

Figure 6. The microstructure of Nimonic 263 after LSP processing by laser energy of 25 mJ and wavelength of 532 nm (power density 2.6 GW/cm^2), and number of pulses 50 (**A**); 100 (**B**) and 200 (**C**).

As the higher number of pulses and pulse energy caused unfavorable "coral" structure formation, the best results, for the material processing at 532 nm, are considered to be for 50 number of pulses and 25 mJ pulse energy action. Characteristic microstructures and microconstituents arisen after picosecond LSP with the laser wavelength of 532 nm, laser beam energy of 25 mJ and 50 laser beam pulses are shown in Figure 7. Corresponding EDS analysis listed in Table 5 shows the presence of oxygen in Figure 7a and suggests that oxides are formed. The creation of different grains can be noticed in Figure 7b. The grain boundaries are clearly pronounced. Some of the grains consist of many pores, sized up to 1.2 µm. Figure 7c shows the twins arisen by deformation induced by mechanical treatment of the surface. Due to the high strain rates involved in the laser shock peening process, the shock waves induce plastic deformation, through the sliding and deformation hardening, which results in twins' formation.

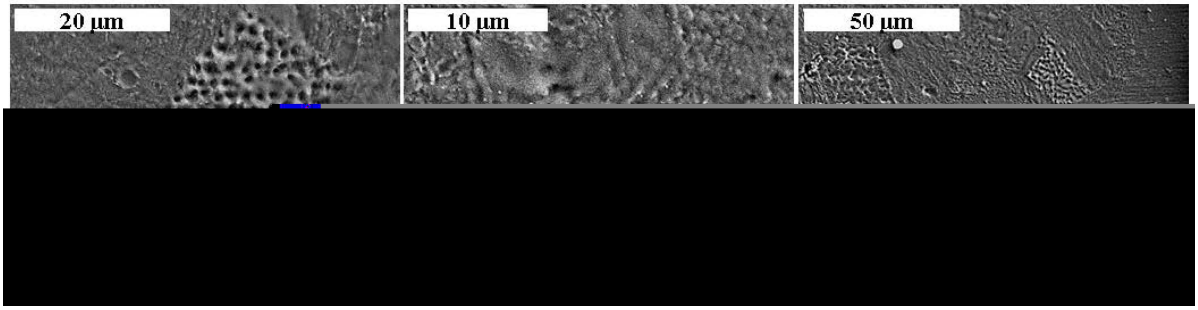

Figure 7. Nimonic 263 surface, processed by laser energy of 25 mJ at wavelength of 532 nm and 50 accumulated pulses (power density 2.4 GW/cm^2): (**A**) microstructure; (**B**) grains; and (**C**) twinned grains.

Table 5. EDS analysis of the area presented in Figure 7a and the spots shown in Figure 7b.

Spectrum	C	O	Al	Si	Ti	Cr	Mn	Fe	Co	Ni	Mo
Figure 7a	11.49	6.92	0.28	0.23	1.58	15.59	0.45	0.43	16.69	41.79	4.57
Spectrum 1	13.25	-	0.13	0.2	25.94	9.66	0.34	0.24	8.82	21.98	19.45
Spectrum 2	12.96	-	0.18	0.25	20.15	11.50	0.37	0.29	11.12	27.43	15.77

Table 5 presents EDS results of the whole area shown in Figure 7a, and the spectrums presented in Figure 7b. In Figure 7a, degasation is noticed in some of the grains, and EDS analysis shows the higher content of carbon and oxide due to mechanism of the process. The presence of the triple grain boundary is presented in Figure 7b. The EDS results presented in Table 5 show the high content of Ti and Mo and, along with the morphology, suggest that the (TiMo) carbides are formed. The size of these carbides is up to 2 µm. At the grain boundaries the carbides are in the favorable form of chain, with higher hardness [34].

Alloy materials usually have some special mechanical and physical characteristics under high strain rates; their structures may generate dislocation, grains and twins, as it was presented by Ren *et al.* [35]. In Figure 7c, the twinned grains are noticed, formed due to the mechanical treatment of a material. As was discussed by Matijasevic *et al.* [29], the twinned grains have been formed at the high stress concentration when the large number of barriers interferes with the dislocation movement. As the dislocations pile up at obstacles in local area, the lattice strain increases. Internal stresses are added on the outside ones and cause formation of the twinned grain. It is well known that all face-centered cubic (FCC) metals, under the action of impact load (high strain rate), can be deformed by twinning [29].

3.3. Comparison of Results Obtained by Laser Operating at 1064 nm and 532 nm

Figure 8a–c presents the microstructures of the base material and laser shock peened surface by 1064 nm and 532 nm light, respectively.

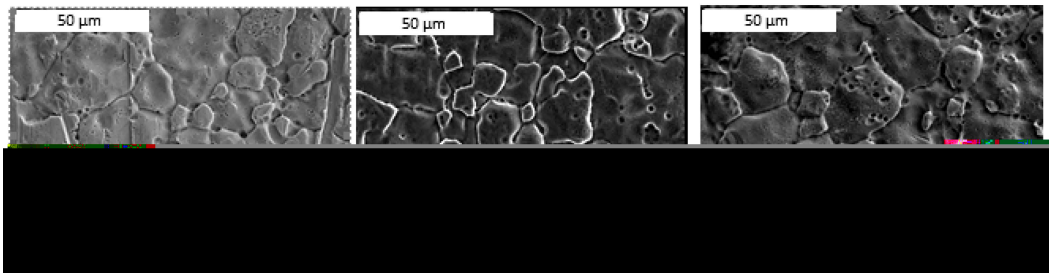

Figure 8. The microstructures of Nimonic 263, recorded by SEM: (**A**) base material; (**B**) laser treated material with 1064 nm, 50 pulses, 10 mJ (power density 3.3 GW/cm^2); and (**C**) laser treated material with 532 nm, 50 pulses, 25 mJ.

After laser shock peening by picosecond laser the microstructure is finer (the grains are smaller) and more uniform. The finest structure with the average grain size *F*m = 163.24 µm^2 is obtained by the following process parameters: pulse energy of 10 mJ, 50 pulses and wavelength of 1064 nm (Figure 8b).

The above shown microstructural changes introduced by the optimized LSP may cause improvements of mechanical properties such as hardness, tensile strength, and fatigue strength, as it was previously discussed by Warren *et al.* [36] and Ren *et al.* [35].

In Table 6, the estimated values of peak pressure are presented for energy at 532 nm and at 1064 nm wavelength. The laser pulse diameter at the Nimonic surface is ~1.6 mm for 1064 nm wavelength and ~3 mm for 532 nm beam. Laser fluence is calculated by dividing laser energy (mJ) and modified surface area (cm^2). For the calculated fluences and pulse duration of 150 ps, the values presented in Table 6 are obtained using the formula: $P\,(\mathrm{GPa}) = \sqrt{I_0}(\mathrm{GW/cm^2})$ in water-confined ablation mode [16,37].

Table 6. Estimated values of peak pressure for different pulse energies at two different wavelength.

Wavelength (nm)	**532**			**1064**		
Pulse energy (mJ)	25	30	35	2	10	15
Power density(GW/cm^2)	0.6	3.3	5.0	1.9	2.4	2.8
Peak pressure (GPa)	2.2	2.4	2.7	1.3	2.9	3.6

Surface morphology/topography plays an important role in the performance of parts of various machines. Surface roughness implies that the surface is not perfectly flat, and consequently, small sized stress concentrations along the material surface occur. Under fatigue loading, cracks always nucleate from the free surface. Cracks nucleate at positions where the plastic strain concentrations are high. High surface roughness generates local stress concentration and accelerates crack initiation. For wear resistance applications, removal of the roughened surface is necessary, as previously shown by Grinspan and Gnanamoorthy [38]. This is why a significant part of this research was dedicated to the surface roughness analysis.

Two-dimensional profiles and 3D maps of the areas after LSP processing at both wavelengths and after 50 accumulated pulses are presented in Figure 9. The noncontact profilometry measurements are based on the interference between white light reflected from the sample surface and the reference surface.

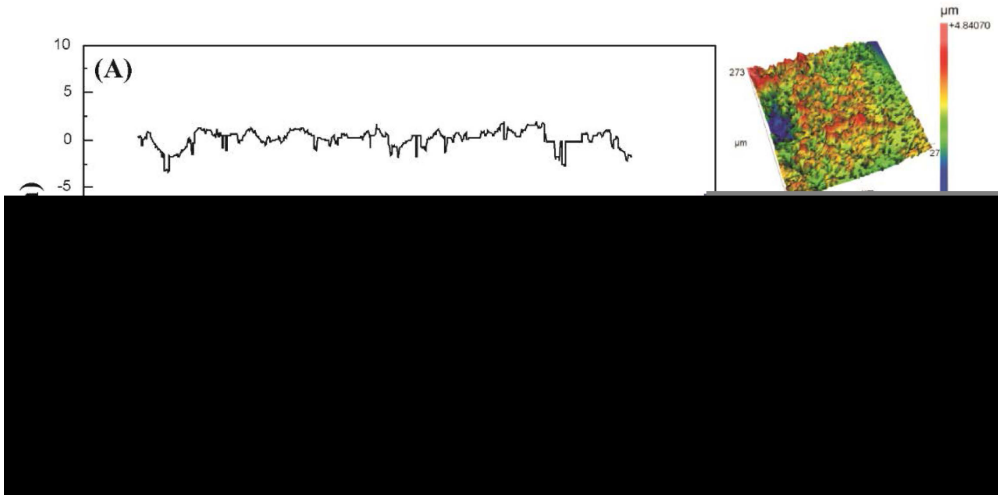

Figure 9. 3D maps and 2D profiles of the areas modified with 50 accumulated laser pulses: (**A**) at 1064 nm wavelength and output laser energy of 10 mJ (power density 3.3 GW/cm^2); and (**B**) at 532 nm wavelength and pulse laser energy of 25 mJ.

Two-dimensional surface profiles show that LSP processing of the alloy surface caused relatively homogeneous modification of the surface throughout the interaction area, as shown in Figure 9. No significant ablation or hydrodynamic effects were detected due to low value of fluence and presence of the protective black paint.

Generally, LSP modifies the surface and accordingly, surface parameters of the non-irradiated sample. For more detailed analysis, the effect of process conditions on the surface parameters is presented in Figure 10. Figure 10a,b shows the influence of pulse energy and wavelength on the average roughness (R_a) and peak to valley (PV) ratio, respectively.

Figure 10. Diagrams of Nimonic 263 surface morphology parameters with respect to the laser energy, after 50 accumulated pulses: (**A**) average roughness (R_a) and (**B**) peak to valley (PV) ratio.

Diagram in Figure 10a shows that the main increase of the R_a value is after 25 mJ laser action at 532 nm. With additional increase of laser energy, the average surface roughness is decreasing. Analysis of the results of surface parameters with an increase in the number of pulses shows that there are no significant changes in the R_a value; therefore, they are not discussed further. Concerning PV ratio, the profilometry analysis shows slight fluctuations of PV ratio with an increase of the pulse energy at 1064 nm, as it could be seen from Figure 10b. At 532 nm laser action, the descending trend of PV ratio is noticed when higher energy is applied (Figure 10b).

Hardening effect is expected to be present after surface treatment by the laser light. The results of microhardness measurement (HV0.5) for the base material (BM) and the material treated by laser process parameters: wavelength at 1064 nm, $E1$ = 2 mJ, $E2$ = 10 mJ and $E3$ = 15 mJ, and the number of pulses 50, 100 and 200, are given in Figure 11.

As can be observed in Figure 11, at the experimental conditions of low fluence laser irradiation of the Nimonic 263 alloy, there are no significant variations in the microhardness values between different irradiated areas of the sample. But, comparing with the non-irradiated sample, there is an overall increase of microhardness due to LSP processing. There is a relationship between the hardness and the strength of austenitic materials, where normally the hardness increases while the strength increases, and the ductility decreases.

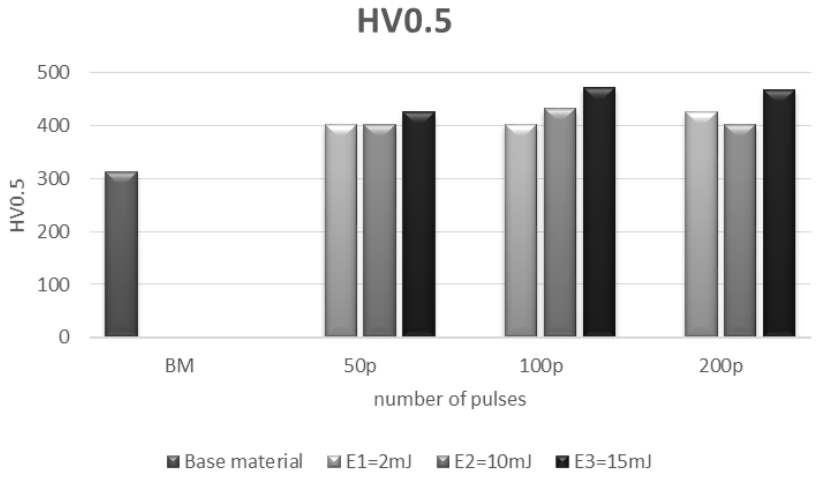

Figure 11. The microhardness measurements of LSP processed areas by laser energies: $E1$ = 2 mJ, $E2$ = 10 mJ and $E3$ = 15 mJ, at wavelength 1064 nm.

Figure 12 presents the microhardness values of the material treated by the following laser process parameters: wavelength at 532 nm; $E1$ = 25 mJ, $E2$ = 30 mJ and $E3$ = 35 mJ; and the number of pulses 50, 100 and 200. Comparing Figures 11 and 12 it can be concluded that laser beam wavelength does not significantly affect the microhardness values. Figure 13 shows the microhardness measurements of areas treated by laser energy of 25 mJ and number of pulses 50 and 100, at wavelength 532 nm. As can be seen in the graph, the microhardness value slightly decreases in depth as the influence of shock waves is fading away.

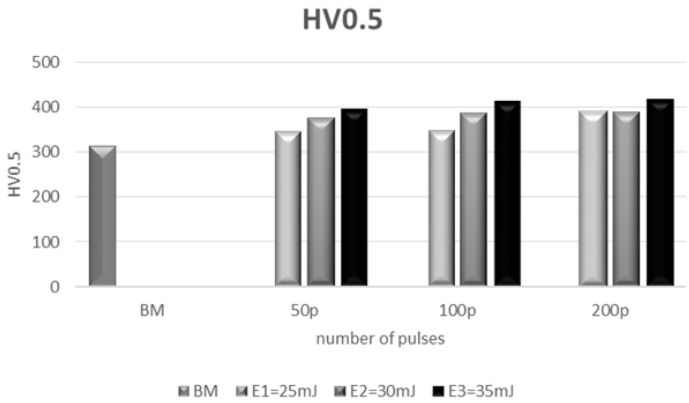

Figure 12. The microhardness measurements of LSP processed areas by laser energies: $E1$ = 25 mJ, $E2$ = 30 mJ and $E3$ = 35 mJ, at wavelength 532 nm.

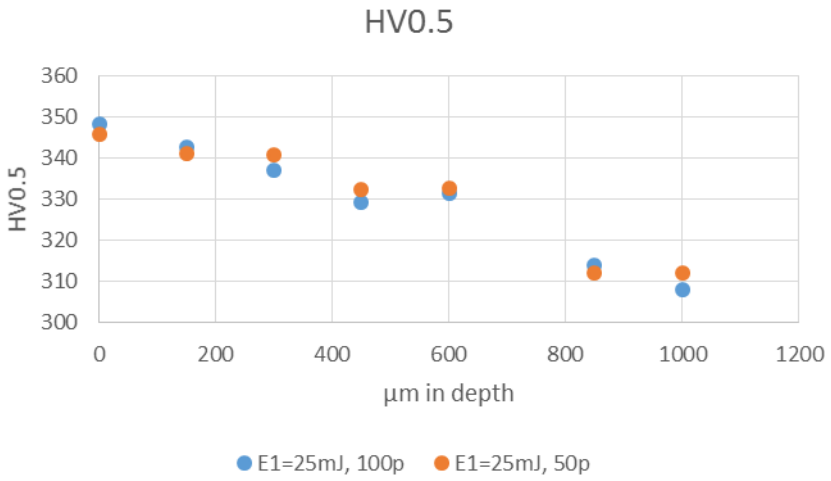

Figure 13. The microhardness measurments in depth of LSP areas treated by laser energy $E1$ = 25 mJ and number of pulses 50 and 100, at wavelength 532 nm.

4. Conclusions

In this paper, the surface microstructural changes of superalloy Nimonic 263 induced by picosecond laser mechanical treatment were discussed. Laser shock peening was performed in different regimes. Special attention was dedicated to the effects of 532 nm and 1064 nm wavelength laser treatments. The following conclusions can be drawn from this study.

After LSP by picosecond laser, the microstructure is finer (the grains are smaller) and more uniform, compared to the base material.

The laser action at two different wavelengths has different impact on material characteristics/morphology/surface. The laser at 1064 nm wavelength produces finer structure and lower roughness than the laser action at 532 nm wavelength. At both wavelengths, LSP processing induced favorable phases, but during 1064 nm treatment unwanted phases, Ti carbides, occurred that might cause initiation of crack formation.

At wavelength 532 nm, with an increase in pulse energy and number of accumulated pulses, the pores start to form and create a coral-like structure. The grain boundaries are more pronounced, they start to segregate, and carbides are formed at the grain boundaries.

At wavelength 1064 nm, the finest structure is obtained for pulse energy 10 mJ, while the further increase in energy causes the formation of pores. By increasing the pulse numbers, the grains become finer; however, at 200 pulses, melting occurs.

Overall, picosecond LSP treatment of Nimonic 263 improved microhardness of superalloy's surface. These results show that LSP by picosecond laser presents a promising technique for superalloy's surface processing, which aims to obtain beneficial mechanical characteristics of the observed material.

Further research might include residual stresses measurements and analysis, as well as the investigation of the same process using different lasers and processing different materials.

Acknowledgments: The work was supported by the Ministry of Education and Science of the Republic of Serbia, under grant numbers TR 35040 and ON 172019.

Author Contributions: S. Petronic and M. Burzic conceived and designed the experiments; S. Polic performed the experiments; T. Sibalija and K. Colic analyzed the data; D. Milovanovic contributed materials and analysis tools; and S. Petronic and T. Sibalija wrote the paper.

Conflicts of Interest: The authors declare no conflict of interest.

References

1. Pollock, M.T.; Tin, S. Nickel-Based Superalloys for Advanced Turbine Engines: Chemistry, Microstructure, and Properties. *J. Propuls. Power* **2006**, *22*, 361–374. [CrossRef]
2. Shahriari, D.; Sadeghi, M.H.; Akbarzadeh, A.; Cheraghzade, M. The influence of heat treatment and hot deformation conditions on γ' precipitate dissolution of Nimonic 115 superalloy. *J. Adv. Manuf. Technol.* **2009**, *45*, 841–850. [CrossRef]
3. Singh, P.N.; Singh, V. Influence of ageing treatment on work hardening behavior of Ni-base superalloy. *Scr. Mater.* **1996**, *34*, 1861–1865. [CrossRef]
4. Park, N.K.; Kim, I.S.; Na, Y.S.; Yeom, J.T. Hot forging of a nickel-base superalloy. *J Mater. Process. Technol.* **2001**, *111*, 98–102. [CrossRef]
5. Milovanovic, D.S.; Radak, B.B.; Gakovic, B.M.; Batani, D.; Momcilovic, M.D.; Trtica, M.S. Surface morphology modifications of titanium based implant induced by 40 picosecond laser pulses at 266 nm. *J. Alloy Compd.* **2010**, *501*, 89–92. [CrossRef]
6. Petronic, S.; Milovanovic, D.; Milosavljevic, A.; Momcilovic, M.; Petrusko, D. Influence of picosecond laser irradiation on nickel-based superalloy surface microstructure. *Phys Scr.* **2012**. [CrossRef]
7. Yilbas, B.S.; Shuja, S.Z.; Arif, A.; Gondal, M.A. Laser-shock processing of steel. *J. Mater. Proc. Technol.* **2003**, *135*, 6–17. [CrossRef]
8. Peyre, P.; Fabbro, R. Laser shock processing: A review of the physics and applications. *Opt. Quantum Electr.* **1995**, *27*, 1213–1229.
9. Devaux, D.; Fabbro, R.; Tollier, L.; Bartnicki, E. Generation of shock waves by laser-induced plasma in confined geometry. *J. Appl. Phys.* **1993**, *74*, 2268–2273. [CrossRef]
10. Peyre, P.; Fabbro, R.; Berthe, L.; Dubouchet, C. Laser shock processing of materials, physical processes involved and examples of application. *J. Laser Appl.* **1996**, *8*, 135–141. [CrossRef]
11. Zhong, H.; Yu, C. Laser shock processing of 2024-T62 aluminum alloy. *Mater. Sci. Eng. A* **1998**, *257*, 322–327.
12. Clauer, A.H.; Holbrook, J.H.; Fairand, B.P. Effects of laser induced shock waves. In *Shock Waves and High-Strain, Phenomena in Metals*; Meyers, M.A., Murr, L.E., Eds.; Plenum Press: New York, NY, USA, 1981; pp. 675–703.
13. Amarchinta, H.K.; Grandhi, R.V.; Clauer, A.H.; Langer, K.; Stargel, D.S. Simulation of residual stress induced by a laser peening process through inverse optimization of material models. *J. Mater. Process. Technol.* **2010**, *210*, 1997–2006. [CrossRef]
14. Peyre, P.; Chaieb, I.; Braham, C. FEM calculation of residual stresses induced by laser shock processing in stainless steels. *Model. Simul. Mater. Sci. Eng.* **2007**, *15*, 205–221. [CrossRef]
15. Sibalija, T.; Petronic, S.; Majstorovic, V.; Milosavljevic, A. Modelling and optimisation of laser shock peening using an integrated simulated annealing-based method. *Int. J. Adv. Manuf. Technol.* **2014**, *73*, 1141–1158. [CrossRef]
16. Ding, K.; Ye, L. *Laser Shock Peening, Performance and Process Simulation*; Woodhead Publishing Limited: Cambridge, UK, 2006; pp. 50–53.
17. Schijve, J. *Fatigue of Structures and Materials*; Kluwer Academic Publisher: Dordrecth, The Netherlands, 2001; pp. 71–78.
18. Lee, D. Feasibility Study on Laser Microwelding and Laser Shock Peening Using Femtosecond Laser Pulses. Ph.D. Thesis, University of Michigen, Ann Arbor, MI, USA, 2008.
19. Semaltianos, N.G.; Perrie, W.; French, P.; Sharp, M.; Dearden, G.; Logothetidis, S.; Watkins, K.G. Femtosecond laser ablation characteristics of nickel-based superalloy C263. *Appl. Phys. A* **2009**, *94*, 999–1009. [CrossRef]
20. Gomez-Rosas, G.; Rubio-Gonzalez, C.; Ocaña, J.L.; Molpeceres, C.; Porro, J.A.; Morales, M.; Casillas, F.J. Laser Shock Processing of 6061-T6 Al alloy with 1064 nm and 532 nm wavelengths. *Appl. Surf. Sci.* **2010**, *256*, 5828–5831. [CrossRef]
21. Schumann, H. *Metallographie*; Deutscher Verlag fuer Grundstoffindustrie: Leipzig, Germany, 1974; p. 15.
22. Petronic, S.; Burzic, M.; Milovanovic, D.; Colic, K.; Radovanovic, Z. Picosecond laser shock peening of base material Nimonic 263 material and laser welded Nimonic 263 alloy. *Weld. Weld. Struct.* **2015**, *60*, 149–155.
23. Petronic, S.; Kovacevic, A.G.; Milosavljevic, A.; Sedmak, A. Microstructural changes of Nimonic 263 superalloy caused by laser beam action. *Phys. Scr.* **2012**. [CrossRef]
24. Bauerle, D. *Laser Processing and Chemistry*; Springer Verlag: Berlin, Germany, 2003; pp. 13–256.

25. Peyre, P.; Berthe, L.; Scherpereel, X.; Fabbro, R.; Bartniki, E. Experimental Study of Laser-Driven Shock Waves in Stainless Steels. *J. Appl. Phys.* **1998**, *84*, 5985–5992. [CrossRef]
26. Niehofff, H.S.; Vollertsen, F. Laser induced shock waves in deformation processing. *J. Metall.* **2005**, *11*, 183–194.
27. Berthe, L.; Fabbro, R.; Peyre, P.; Tollier, L.; Bartnicki, E. Shock waves from a water-confined laser-generated plasma. *J. Appl. Phys.* **1997**, *82*, 2826–2832. [CrossRef]
28. Drobnjak. *Physical metallurgy*; Faculty of Technology and Metallurgy, University of Belgrade: Belgrade, Serbia, 1981; pp. 75–77.
29. Matijasevic, B.; Kinder, J.; Radovic, N.A.; Volkov-Husovic, T. Shot-peening induced twinning in ship-building steel. *Metalurgija* **2002**, *8*, 149–155.
30. Zhang, Y.K.; Lu, J.Z.; Ren, X.D.; Yao, H.B.; Yao, H.X. Effect of laser shock processing on the mechanical properties and fatigue lives of the turbojet engine blades manufactured by LY2 aluminum alloy. *Mater. Des.* **2009**, *30*, 1697–1703. [CrossRef]
31. Schneider, M.S.; Kad, B.; Kalantar, D.H.; Remington, B.A.; Kenik, E.; Jarmakani, H.; Meyers, M.A. Laser shock compression of copper and copper-aluminum alloys. *Int. J. Impact Eng.* **2005**, *32*, 473–507. [CrossRef]
32. Reed, R. *The Superalloys—Fundamentals and Applications*; Cambridge University Press: New York, NY, USA, 2006.
33. Chena, C.Y.; Yena, H.W.; Kaoa, F.H.; Li, W.C.; Huang, C.Y.; Yanga, J.R.; Wang, S.H. Precipitation hardening of high-strength low-alloy steels by nanometer-sized carbides. *Mater. Sci. Eng. A* **2009**, *499*, 162–166. [CrossRef]
34. Jang, J.H.; Lee, C.H.; Heo, Y.U.; Suh, D.H. Stability of (Ti, *M*)C (*M* = Nb, V, Mo and W) Carbide in Steels using First-Principles Calculations. *Acta Mater.* **2012**, *60*, 208–217. [CrossRef]
35. Ren, X.D.; Zhang, Y.K.; Zhang, T.; Jiang, D.W.; Yongzhuo, H.F.; Jiang, Y.F.; Chen, K.M. Comparison of the simulation and experimental fatigue crack behaviours in the nanoseconds laser shocked aluminum alloy. *Mater. Des.* **2011**, *32*, 1138–1143. [CrossRef]
36. Warren, A.W.; Guo, Y.B.; Chen, S.C. Massive parallel laser shock peening: Simulation, analysis, and validation. *Int. J. Fatigue* **2008**, *30*, 188–197. [CrossRef]
37. Fabbro, R.; Fournier, J.; Ballard, P.; Devaux, D.; Virmont, J. Physical study of laser-produced plasma in confined geometry. *J. Appl. Phys.* **1990**. [CrossRef]
38. Grinspan, A.S.; Gnanamoorthy, R. Surface modification by oil jet peening in Al alloys, AA6063-T6 and AA6061-T4 Part 2: Surface morphology, erosion, and mass loss. *Appl. Surf. Sci.* **2006**, *253*, 997–1005. [CrossRef]